JACS
JOURNAL OF THE AMERICAN CHEMICAL SOCIETY

pubs.acs.org/JACS

Communication

Role of Water in $CaCO_3$ Biomineralization

Hao Lu,* Yu-Chieh Huang, Johannes Hunger, Denis Gebauer, Helmut Cölfen, and Mischa Bonn*

Cite This: *J. Am. Chem. Soc.* 2021, 143, 1758−1762

Read Online

ACCESS | Metrics & More | Article Recommendations | Supporting Information

ABSTRACT: Biomineralization occurs in aqueous environments. Despite the ubiquity and relevance of $CaCO_3$ biomineralization, the role of water in the biomineralization process has remained elusive. Here, we demonstrate that water reorganization accompanies $CaCO_3$ biomineralization for sea urchin spine generation in a model system. Using surface-specific vibrational spectroscopy, we probe the water at the interface of the spine-associated protein during $CaCO_3$ mineralization. Our results show that, while the protein structure remains unchanged, the structure of interfacial water is perturbed differently in the presence of both Ca^{2+} and CO_3^{2-} compared to the addition of only Ca^{2+}. This difference is attributed to the condensation of prenucleation mineral species. Our findings are consistent with a nonclassical mineralization pathway for sea urchin spine generation and highlight the importance of protein hydration in biomineralization.

Calcium carbonate ($CaCO_3$) is an abundant bio- and geomineral on Earth and is highly relevant to the environment, being a significant repository of carbon dioxide (CO_2).[1] Knowledge of the mechanism of $CaCO_3$ nucleation is of central importance for the fabrication of bioinspired materials and CO_2 sequestration. So far, much progress has been made in our understanding of the mechanism for *inorganic* $CaCO_3$ generation.[2−5] It has recently been argued that the nucleation of $CaCO_3$ involves stable prenucleation species, i.e., prenucleation ion clusters (PNCs)[2,6,7] or a metastable liquid condensed phase.[8,9] Water plays a key role in the mineralization: the release of water molecules from hydrated mineral ions results in the formation and stabilization of PNCs and, later, in their dehydration and transformation into metastable dense liquid and amorphous intermediates, thereby kinetically directing the mineralization pathway.[6,9−12] This nonclassical nucleation pathway remains debated[3,4] but has not been disproven.[5] Rather, the nonclassical nucleation theory unifies various experimental observations, for instance, the liquid mineral intermediates (polymer-induced liquid precursors[8]) for bioinspired material fabrication.[13]

Different from *inorganic* $CaCO_3$ mineralization,[2,5−8] $CaCO_3$ *bio*mineralization in nature is more complex, taking place in the presence of proteins and other biomolecules. The process relies on the concerted interfacial interactions among protein, mineral, and water.[14,15] Despite the available studies,[10,16] it remains unclear whether $CaCO_3$ mineralization by proteins involves prenucleation species (e.g., PNCs) and what is the role of solvent water.

To shed light on the role of water for $CaCO_3$ mineralization by proteins, we focus on one particularly remarkable system in nature—the sea urchin spine. Its hierarchical supramolecular structure and fascinating material properties have intrigued material scientists for decades.[17−19] We probe the water at the interface of a spine-associated protein during $CaCO_3$ mineralization *in situ* using surface-specific vibrational sum frequency generation (SFG) spectroscopy. SFG is a second-order nonlinear spectroscopy, where the signal is only generated at the surface and interface where centrosymmetry is broken.[20−22] Thus, this method provides the vibrational response of the water molecules only at the spine protein interface for $CaCO_3$ mineralization.

We select one specific spine-associated protein SpSM50, which has unique structural motifs: an N-terminal C-type lectin domain and a residual glycine- and proline-rich repeat region.[23] We study the N-terminal C-type lectin domain (abbreviated as SM50-CTL below); this domain has been recognized as being functional in regulating early nucleation stages and subsequent phase transitions of the $CaCO_3$ mineral phase, in this and other proteins.[23,24]

To improve our understanding of $CaCO_3$ mineralization by SM50-CTL proteins, we first perform a potentiometric titration experiment. In this experiment, Ca^{2+} ions are gradually dosed into a 5 μM SM50-CTL solution in 10 mM carbonate buffer (pH 9.0) to initiate the $CaCO_3$ mineralization process.[2,6] The concentration of free Ca^{2+} ions in solution is quantified by a Ca^{2+} ion-selective electrode (see Supporting Information for details). The obtained titration curve (black), as shown in Figure 1A, allows different mineralization regimes to be distinguished: I−III correspond to under-supersaturation at prenucleation (I), supersaturation at prenucleation (II), and nucleation into (amorphous) minerals (III).[10,19,25,26] As a comparison, the titration curve for Ca^{2+} into Tris buffer (green), which cannot trigger mineralization, is also shown and nearly overlaps the curve for dosed Ca^{2+} (red).

Figure 1B illustrates our experimental scheme to investigate the interface of SM50-CTL proteins during $CaCO_3$ mineral-

Received: November 16, 2020
Published: January 20, 2021

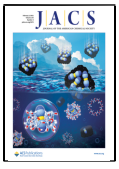

https://dx.doi.org/10.1021/jacs.0c11976
J. Am. Chem. Soc. 2021, 143, 1758−1762

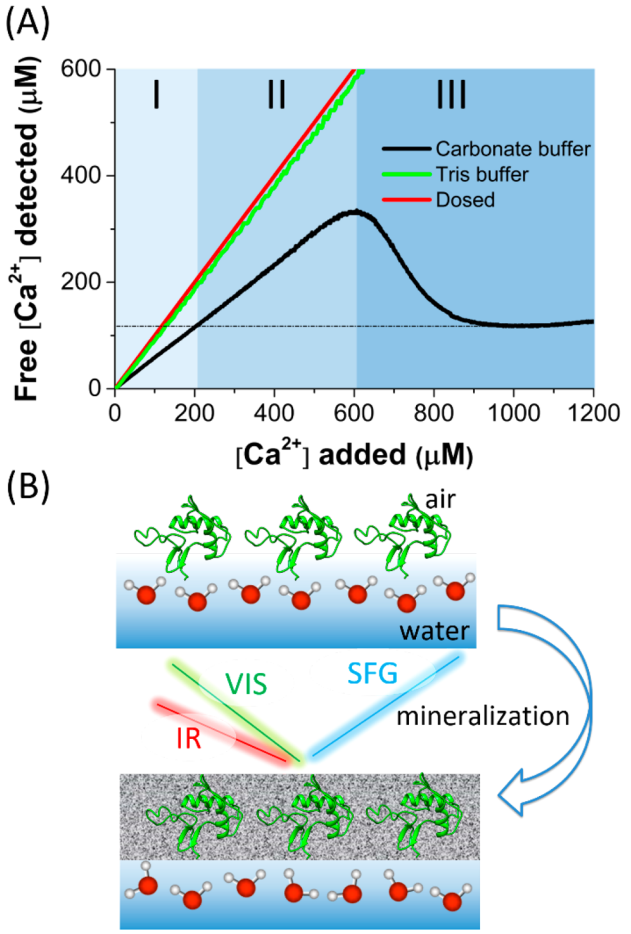

Figure 1. (A) Titration curve of Ca^{2+} into 5 μM SM50-CTL protein in 10 mM carbonate buffer. Different mineralization regimes are marked: under-supersaturation (I), supersaturation (II), and nucleation into (amorphous) minerals (III).[10,19,25,26] The curves for dosed Ca^{2+} (red) and Ca^{2+} titrated into Tris buffer (green) are also shown. (B) Experimental scheme illustrating the interfacial mineralization and SFG spectroscopy. Spectra reported here were recorded with S-, S-, and P-polarized SFG, visible (VIS), and infrared (IR) light, respectively.

ization. The proteins were first allowed to adsorb to the air−carbonate buffer interface. Surface pressure measurement shows the proteins adsorb rapidly to the interface, reaching an equilibrium surface pressure of ∼30 mN/m. The gradual injection of Ca^{2+} has been reported to generate prenucleation $CaCO_3$ species with the size of several nanometers[6,10] and hydrated $CaCO_3$ nuclei at early nucleation.[10] These mineral species, together with Ca^{2+} ions, will screen the protein charge but apparently do not change the surface pressure (Figure S1).[27,28] SFG measurements were performed in parallel with the titration experiment (Figure 1A), allowing the different mineralization stages in the SFG measurement to be probed.

Figure 2A shows the SFG spectra in the amide I region for the SM50-CTL protein assembled at the air−carbonate buffer interface with various Ca^{2+} concentrations. The spectra for the protein in the absence of Ca^{2+} show a distinct band at ∼1665 cm^{-1}, suggesting a well-ordered secondary folding structure at the interface. The response can be adequately described by two sub-bands: one at 1642 cm^{-1}, consistent with a combination of α-helical and β-turn structures,[29,30] and one at 1679 cm^{-1}, pointing to extended β-strands.[29,31] When the Ca^{2+} concentration is varied, no noticeable spectral changes are observed. Accordingly, the inferred amplitudes of the two bands (Figure 2B) also show negligible changes. While a full structural characterization would require elaborate NMR experiments,[32,33] the insensitivity of the amide vibrations points toward negligible conformational changes of the SM50-CTL proteins in the early stage of nucleation, which is further supported by the constant surface pressure (Figure S1) and circular dichroism spectra (Figure S3). The structural components inferred from the CD spectra are consistent with those inferred from SFG.

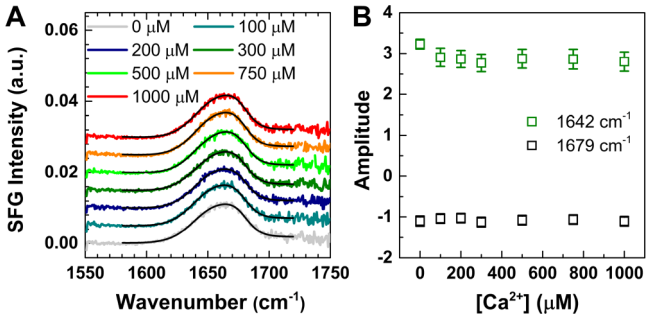

Figure 2. (A) Amide I SFG spectra for SM50-CTL protein at the air−carbonate buffer interface, with various amounts of Ca^{2+} ions indicated in the legend. The fits are shown as black lines. (B) Fitting amplitudes for two amide I bands with different amounts of Ca^{2+}. Error bars represent the standard deviations of amplitudes.

Figure 3A shows the SFG spectra in the CH/OH region for the SM50-CTL protein at the air−carbonate buffer with various Ca^{2+} concentrations. The spectra are dominated by intense OH bands, with peaks at ∼3243 and ∼3432 cm^{-1}, which reflect a distribution of strongly and weakly hydrogen-bonded (H-bonded) OH groups.[22,34] The contribution from protein N−H groups is not discernible in the spectra.[35] The negligible N−H contribution is further supported by the weak chiral PSP SFG signal (Figure S4), to which protein N−H groups and chiral water can contribute.[36,37] The fitted spectra reveal main C−H bands at 2876, 2938, and 3065 cm^{-1},

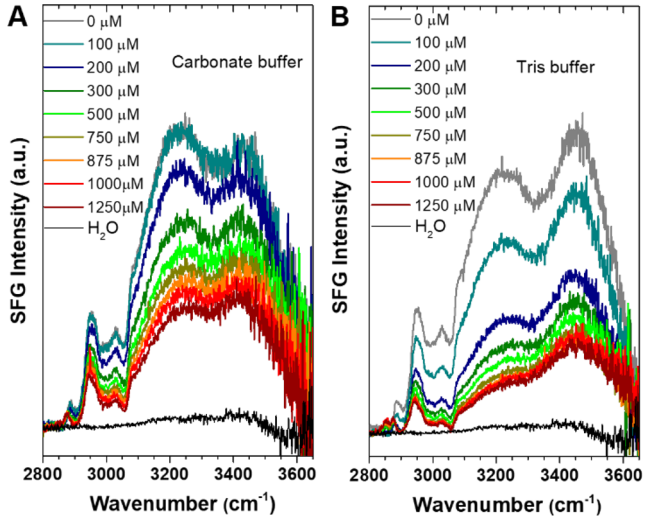

Figure 3. SFG spectra in the CH/OH region for SM50-CTL proteins at the interfaces of air with (A) 10 mM carbonate buffer and (B) 10 mM Tris buffer, at different, indicated Ca^{2+} concentrations. The spectra for pure H_2O are shown for comparison.

https://dx.doi.org/10.1021/jacs.0c11976
J. Am. Chem. Soc. 2021, 143, 1758−1762

attributed to symmetric CH_3 stretch, a combination of CH_3 Fermi resonance and CH_2 stretch from different amino acid side chains,[38,39] and ν_2 modes from aromatic sites,[40] respectively. The observed intensity change of the CH bands upon adding Ca^{2+} ions is caused by interference effects with the changing OH response,[40,41] as confirmed by spectra recorded in isotopically diluted D_2O/H_2O buffer solutions. The CH bands of the protein are unaffected by adding Ca^{2+} ions (Figure S5), in line with the amide I results (Figure 2).

In contrast to the protein amide/CH response, the water response changes substantially with increasing Ca^{2+} concentration. For charged interfaces, the SFG signal of water stems from the interfacial layer ($\chi^{(2)}$ contribution) and the diffuse layer ($\chi^{(3)}$).[42−45] For the moderate ionic strengths used in the present work, the contributions of the diffuse layer dominate, and as such, the SFG intensity of water reports on the surface potential (ϕ_0). Figure 3 shows that, upon addition of Ca^{2+} ions, the water SFG intensity is reduced. Given the constant pH in our experiment (Figure S2), the reduced SFG intensity can stem from neutralization of the negative protein charge or more effective screening of the surface charge due to the increased ionic strength.[27,28,46]

As a reference, we also report SFG spectra for proteins in Tris buffer with the same pH (pH 9) and ionic strength (10 mM) (Figure 3B). Unlike carbonate buffer, the addition of Ca^{2+} ions into Tris buffer cannot induce $CaCO_3$ mineralization. Therefore, this control experiment examines the effect of "pure" charge screening upon adding Ca^{2+} ions. The different spectral lineshapes for proteins in two buffers without Ca^{2+} can be attributed to the different interference between various ($\chi^{(2)}$, $\chi^{(3)}$, and nonresonant) signal sources and/or differences in coupling between OH oscillators.[47] Comparing spectra for pure and isotopically diluted buffers (Figure S6 and S7) reveals such coupling effects but confirms the trends of the changing OH intensity with varying $[Ca^{2+}]$ (Figure S8). As clearly seen in Figure 3, upon adding Ca^{2+} ions, the OH bands decrease in intensity and shift toward higher frequency. The change is more pronounced for the Tris (Figure 3B) than for the carbonate (Figure 3A) buffer.

To quantify the above changes, Figure 4A shows the integrated intensity for the OH bands: $\sum\int_{3100}^{3600} I(\omega)\mathrm{d}\omega$, reflecting the degree of water alignment. Upon adding Ca^{2+} ions to Tris buffer, Σ decreases rapidly; for the carbonate buffer, Σ decreases less dramatically. The weaker response of H-bonded water with Ca^{2+} for carbonate buffer is further supported by quantifying the first moment of the spectral distribution: $\mu = \int_{3100}^{3600}\omega I(\omega)\mathrm{d}(\omega)/\int_{3100}^{3600} I(\omega)\mathrm{d}(\omega)$. Figure 4B shows the change of μ versus $[Ca^{2+}]$ for the two buffers: μ increases much less for the carbonate buffer than for the Tris buffer. After nucleation ($[Ca^{2+}]$ = 1000−1200 μM), the absolute SFG intensity is higher, and μ has changed less for the carbonate buffer than for the Tris buffer. Both observations point to the interfacial water retaining a more ordered structure at the protein interface with $CaCO_3$ than that with only Ca^{2+} cations.

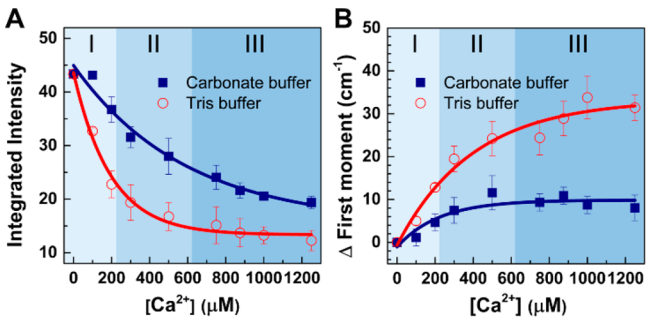

Figure 4. Integrated SFG intensity (A) and change of the first moment (B) of the two OH bands with adding different Ca^{2+} concentrations into carbonate (navy) and Tris buffer (red). The data were all fit to a single-exponential function (shown as lines). The background colors correspond to the different mineralization regimes in accordance with Figure 1A. Error bars show the standard deviations of the integrated intensities from multiple data sets.

The perturbation of interfacial water alignment, as mainly caused by the screening of protein charges, is illustrated in Figure 5. The interfacial water molecules are well-aligned by

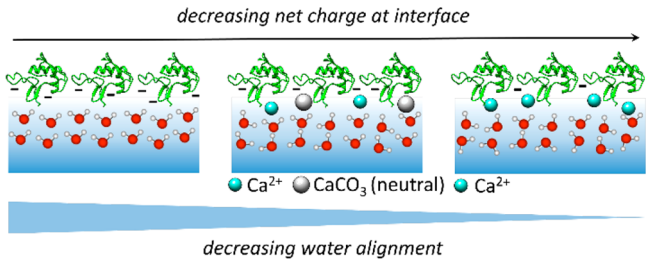

Figure 5. Sketch illustrating decreasing water alignment according to decreasing net charge at the SM50-CTL interface, with (center, carbonate buffer) and without (right, Tris buffer) prenucleation.

the charged proteins; this alignment can be readily perturbed by the screening of the protein charge with Ca^{2+} cations. In the mineralization environment (i.e., carbonate buffer), the charge screening appears less effective, and the first moment indicates that water molecules retain their bulk-like response. The observed water behavior can be rationalized by the co-condensation of other mineralization species, together with Ca^{2+} ions at the interface. Following previous studies on inorganic $CaCO_3$ mineralization,[6,9−12] these species are likely charge-neutral $CaCO_3$ PNCs, which show great protein binding affinity. The presence of neutral PNCs at the protein interface would perturb the water structure, but not so much the alignment, and would explain the relatively rapid change of μ with increasing $[Ca^{2+}]$ while Σ changes more gradually.

Previous experimental[6,10,11] and simulation[9,12] studies state that the stable PNCs further aggregate into nanodroplets in a later prenucleation stage, and the process goes along with water release from the hydration shell and has been related to microscopic liquid−liquid phase separation. This is possibly also relevant for the $CaCO_3$ biomineralization in the presence of SM50-CTL proteins; the largest water perturbations occur in regime II ($[Ca^{2+}]$ = 300−500 μM, Figure 4A), at the point that liquid phase separation may also occur.

In conclusion, surface-specific SFG spectroscopy was applied to probe the SM50-CTL protein and, in particular, water at the interface for mineralization of the sea urchin spine. While the protein structure is unchanged, the structure of interfacial water is perturbed already at prenucleation. The perturbation is caused by the screening of protein charge. However, this screening appears less effective in the presence of carbonate for mineralization than the screening caused by only Ca^{2+} ions, which can be explained by the simultaneous condensation of both $CaCO_3$ and Ca^{2+} to the protein, in line with the formation of PNCs at the protein interface. Our findings

https://dx.doi.org/10.1021/jacs.0c11976
J. Am. Chem. Soc. 2021, 143, 1758−1762

provide evidence for the presence of water in the nonclassical nucleation pathway for mineralization of sea urchin spine. The inferred nonclassical mineralization pathway is possibly relevant for other $CaCO_3$ biominerals.

■ ASSOCIATED CONTENT

Supporting Information

The Supporting Information is available free of charge at https://pubs.acs.org/doi/10.1021/jacs.0c11976.

Details of the experiments and more characterization data: surface pressure, pH variation during titration experiment, circular dichroism, chiral SFG spectra, SFG spectra for experiments in isotopically diluted buffers (PDF)

■ AUTHOR INFORMATION

Corresponding Authors

Hao Lu − *Max Planck Institute for Polymer Research, 55128 Mainz, Germany;* orcid.org/0000-0002-7338-2295; Email: lu@mpip-mainz.mpg.de

Mischa Bonn − *Max Planck Institute for Polymer Research, 55128 Mainz, Germany;* orcid.org/0000-0001-6851-8453; Email: bonn@mpip-mainz.mpg.de

Authors

Yu-Chieh Huang − *Physical Chemistry, Department of Chemistry, University of Konstanz, Konstanz 78464, Germany*

Johannes Hunger − *Max Planck Institute for Polymer Research, 55128 Mainz, Germany;* orcid.org/0000-0002-4419-5220

Denis Gebauer − *Physical Chemistry, Department of Chemistry, University of Konstanz, Konstanz 78464, Germany; Institute of Inorganic Chemistry, Leibniz University of Hannover, 30167 Hannover, Germany;* orcid.org/0000-0003-1612-051X

Helmut Cölfen − *Physical Chemistry, Department of Chemistry, University of Konstanz, Konstanz 78464, Germany;* orcid.org/0000-0002-1148-0308

Complete contact information is available at: https://pubs.acs.org/10.1021/jacs.0c11976

Notes

The authors declare no competing financial interest.

■ ACKNOWLEDGMENTS

We acknowledge financial support from Max Planck Society and the MaxWater Initiative of the Max Planck Society.

■ REFERENCES

(1) Morse, J. W.; Arvidson, R. S.; Luttge, A. Calcium Carbonate Formation and Dissolution. *Chem. Rev.* **2007**, *107*, 342−381.

(2) Gebauer, D.; Kellermeier, M.; Gale, J. D.; Bergstrom, L.; Cölfen, H. Pre-nucleation Clusters as Solute Precursors in Crystallisation. *Chem. Soc. Rev.* **2014**, *43*, 2348−2371.

(3) Smeets, P. J. M.; Finney, A. R.; Habraken, W. J. E. M.; Nudelman, F.; Friedrich, H.; Laven, J.; De Yoreo, J. J.; Rodger, P. M.; Sommerdijk, N. A. J. M. A classical view on nonclassical nucleation. *Proc. Natl. Acad. Sci. U. S. A.* **2017**, *114*, E7882−E7890.

(4) Henzler, K.; Fetisov, E. O.; Galib, M.; Baer, M. D.; Legg, B. A.; Borca, C.; Xto, J. M.; Pin, S.; Fulton, J. L.; Schenter, G. K.; Govind, N.; Siepmann, J. I.; Mundy, C. J.; Huthwelker, T.; De Yoreo, J. J. Supersaturated calcium carbonate solutions are classical. *Sci. Adv.* **2018**, *4*, No. eaao6283.

(5) Gebauer, D.; Raiteri, P.; Gale, J. D.; Cölfen, H. On classical and non-classical views on nucleation. *Am. J. Sci.* **2018**, *318*, 969−988.

(6) Gebauer, D.; Volkel, A.; Cölfen, H. Stable Prenucleation Calcium Carbonate Clusters. *Science* **2008**, *322*, 1819−1822.

(7) Gebauer, D.; Gunawidjaja, P. N.; Ko, J. Y. P.; Bacsik, Z.; Aziz, B.; Liu, L. J.; Hu, Y. F.; Bergstrom, L.; Tai, C. W.; Sham, T. K.; Eden, M.; Hedin, N. Proto-Calcite and Proto-Vaterite in Amorphous Calcium Carbonates. *Angew. Chem., Int. Ed.* **2010**, *49*, 8889−8891.

(8) Gower, L. B.; Odom, D. J. Deposition of calcium carbonate films by a polymer-induced liquid-precursor (PILP) process. *J. Cryst. Growth* **2000**, *210*, 719−734.

(9) Wallace, A. F.; Hedges, L. O.; Fernandez-Martinez, A.; Raiteri, P.; Gale, J. D.; Waychunas, G. A.; Whitelam, S.; Banfield, J. F.; De Yoreo, J. J. Microscopic Evidence for Liquid-Liquid Separation in Supersaturated $CaCO_3$ Solutions. *Science* **2013**, *341*, 885−889.

(10) Sebastiani, F.; Wolf, S. L. P.; Born, B.; Luong, T. Q.; Cölfen, H.; Gebauer, D.; Havenith, M. Water Dynamics from THz Spectroscopy Reveal the Locus of a Liquid-Liquid Binodal Limit in Aqueous $CaCO_3$ Solutions. *Angew. Chem., Int. Ed.* **2017**, *56*, 490−495.

(11) Kellermeier, M.; Raiteri, P.; Berg, J. K.; Kempter, A.; Gale, J. D.; Gebauer, D. Entropy Drives Calcium Carbonate Ion Association. *ChemPhysChem* **2016**, *17*, 3535−3541.

(12) Raiteri, P.; Gale, J. D. Water Is the Key to Nonclassical Nucleation of Amorphous Calcium Carbonate. *J. Am. Chem. Soc.* **2010**, *132*, 17623−17634.

(13) Berg, J. K.; Jordan, T.; Binder, Y.; Borner, H. G.; Gebauer, D. Mg^{2+} Tunes the Wettability of Liquid Precursors of $CaCO_3$: Toward Controlling Mineralization Sites in Hybrid Materials. *J. Am. Chem. Soc.* **2013**, *135*, 12512−12515.

(14) Mann, S. *Biomineralization: Principles and Concepts in Bioinorganic Materials Chemistry*; Oxford University Press: Oxford, 2001.

(15) Mao, L. B.; Gao, H. L.; Yao, H. B.; Liu, L.; Cölfen, H.; Liu, G.; Chen, S. M.; Li, S. K.; Yan, Y. X.; Liu, Y. Y.; Yu, S. H. Synthetic nacre by predesigned matrix-directed mineralization. *Science* **2016**, *354*, 107−110.

(16) Du, H. C.; Amstad, E. Water: How Does It Influence the CaCO3 Formation? *Angew. Chem., Int. Ed.* **2020**, *59*, 1798−1816.

(17) Seto, J.; Ma, Y. R.; Davis, S. A.; Meldrum, F.; Gourrier, A.; Kim, Y. Y.; Schilde, U.; Sztucki, M.; Burghammer, M.; Maltsev, S.; Jager, C.; Cölfen, H. Structure-property relationships of a biological mesocrystal in the adult sea urchin spine. *Proc. Natl. Acad. Sci. U. S. A.* **2012**, *109*, 3699−3704.

(18) Killian, C. E.; Metzler, R. A.; Gong, Y. U. T.; Olson, I. C.; Aizenberg, J.; Politi, Y.; Wilt, F. H.; Scholl, A.; Young, A.; Doran, A.; Kunz, M.; Tamura, N.; Coppersmith, S. N.; Gilbert, P. U. P. A. Mechanism of Calcite Co-Orientation in the Sea Urchin Tooth. *J. Am. Chem. Soc.* **2009**, *131*, 18404−18409.

(19) Politi, Y.; Metzler, R. A.; Abrecht, M.; Gilbert, B.; Wilt, F. H.; Sagi, I.; Addadi, L.; Weiner, S.; Gilbert, P. U. P. A. Transformation mechanism of amorphous calcium carbonate into calcite in the sea urchin larval spicule. *Proc. Natl. Acad. Sci. U. S. A.* **2008**, *105*, 17362−17366.

(20) Lambert, A. G.; Davies, P. B.; Neivandt, D. J. Implementing the Theory of Sum Frequency Generation Vibrational Spectroscopy: A Tutorial Review. *Appl. Spectrosc. Rev.* **2005**, *40*, 103−145.

(21) Shen, Y. R. *The Principles of Nonlinear Optics*; Wiley: New York, 1984.

(22) Bonn, M.; Nagata, Y.; Backus, E. H. G. Molecular Structure and Dynamics of Water at the Water-Air Interface Studied with Surface-Specific Vibrational Spectroscopy. *Angew. Chem., Int. Ed.* **2015**, *54*, 5560−5576.

(23) Wilt, F. H. Biomineralization of the Spicules of Sea Urchin Embryos. *Zool. Sci.* **2002**, *19*, 253−261.

(24) Rao, A.; Roncal-Herrero, T.; Schmid, E.; Drechsler, M.; Scheffner, M.; Gebauer, D.; Kroger, R.; Cölfen, H. On Biomineraliza-

tion: Enzymes Switch on Mesocrystal Assembly. *ACS Cent. Sci.* **2019**, *5*, 357−364.
(25) Avaro, J. T.; Wolf, S. L. P.; Hauser, K.; Gebauer, D. Stable Prenucleation Calcium Carbonate Clusters Define Liquid−Liquid Phase Separation. *Angew. Chem., Int. Ed.* **2020**, *59*, 6155−6159.
(26) Beniash, E.; Aizenberg, J.; Addadi, L.; Weiner, S. Amorphous calcium carbonate transforms into calcite during sea urchin larval spicule growth. *Proc. R. Soc. London, Ser. B* **1997**, *264*, 461−465.
(27) Schabes, B. K.; Altman, R. M.; Richmond, G. L. Come Together: Molecular Details into the Synergistic Effects of Polymer−Surfactant Adsorption at the Oil/Water Interface. *J. Phys. Chem. B* **2018**, *122*, 8582−8590.
(28) Bilkova, E.; Pleskot, R.; Rissanen, S.; Sun, S.; Czogalla, A.; Cwiklik, L.; Rog, T.; Vattulainen, I.; Cremer, P. S.; Jungwirth, P.; Coskun, U. Calcium Directly Regulates Phosphatidylinositol 4,5-Bisphosphate Headgroup Conformation and Recognition. *J. Am. Chem. Soc.* **2017**, *139*, 4019−4024.
(29) Nguyen, K. T.; King, J. T.; Chen, Z. Orientation Determination of Interfacial β-Sheet Structures in Situ. *J. Phys. Chem. B* **2010**, *114*, 8291−8300.
(30) Chen, X. Y.; Wang, J.; Sniadecki, J. J.; Even, M. A.; Chen, Z. Probing α-Helical and β-Sheet Structures of Peptides at Solid/Liquid Interfaces with SFG. *Langmuir* **2005**, *21*, 2662−2664.
(31) Hilario, J.; Kubelka, J.; Keiderling, T. A. Optical Spectroscopic Investigations of Model β-Sheet Hairpins in Aqueous Solution. *J. Am. Chem. Soc.* **2003**, *125*, 7562−7574.
(32) Weidner, T.; Breen, N. F.; Li, K.; Drobny, G. P.; Castner, D. G. Sum frequency generation and solid-state NMR study of the structure, orientation, and dynamics of polystyrene-adsorbed peptides. *Proc. Natl. Acad. Sci. U. S. A.* **2010**, *107*, 13288−13293.
(33) Buckle, E. L.; Prakash, A.; Bonomi, M.; Sampath, J.; Pfaendtner, J.; Drobny, G. P. Solid-State NMR and MD Study of the Structure of the Statherin Mutant SNa15 on Mineral Surfaces. *J. Am. Chem. Soc.* **2019**, *141*, 1998−2011.
(34) Du, Q.; Freysz, E.; Shen, Y. R. Surface Vibrational Spectroscopic Studies of Hydrogen Bonding and Hydrophobicity. *Science* **1994**, *264*, 826−828.
(35) Meister, K.; Paananen, A.; Bakker, H. J. Identification of the response of protein N−H vibrations in vibrational sum-frequency generation spectroscopy of aqueous protein films. *Phys. Chem. Chem. Phys.* **2017**, *19*, 10804−10807.
(36) Yan, E. C. Y.; Wang, Z. G.; Fu, L. Proteins at Interfaces Probed by Chiral Vibrational Sum Frequency Generation Spectroscopy. *J. Phys. Chem. B* **2015**, *119*, 2769−2785.
(37) Perets, E. A.; Yan, E. C. Y. The H_2O Helix: The Chiral Water Superstructure Surrounding DNA. *ACS Cent. Sci.* **2017**, *3*, 683−685.
(38) Watry, M. R.; Richmond, G. L. Orientation and Conformation of Amino Acids in Monolayers Adsorbed at an Oil/Water Interface As Determined by Vibrational Sum-Frequency Spectroscopy. *J. Phys. Chem. B* **2002**, *106*, 12517−12523.
(39) Holinga, G. J.; York, R. L.; Onorato, R. M.; Thompson, C. M.; Webb, N. E.; Yoon, A. P.; Somorjai, G. A. An SFG Study of Interfacial Amino Acids at the Hydrophilic SiO2 and Hydrophobic Deuterated Polystyrene Surfaces. *J. Am. Chem. Soc.* **2011**, *133*, 6243−6253.
(40) Engelhardt, K.; Peukert, W.; Braunschweig, B. Vibrational sum-frequency generation at protein modified air−water interfaces: Effects of molecular structure and surface charging. *Curr. Opin. Colloid Interface Sci.* **2014**, *19*, 207−215.
(41) Lukas, M.; Schwidetzky, R.; Kunert, A. T.; Poschl, U.; Frohlich-Nowoisky, J.; Bonn, M.; Meister, K. Electrostatic Interactions Control the Functionality of Bacterial Ice Nucleators. *J. Am. Chem. Soc.* **2020**, *142*, 6842−6846.
(42) Ohno, P. E.; Wang, H.-F.; Geiger, F. Second-order spectral lineshapes from charged interfaces. *Nat. Commun.* **2017**, *8*, 1032.
(43) Pullanchery, S.; Yang, T. L.; Cremer, P. S. Introduction of Positive Charges into Zwitterionic Phospholipid Monolayers Disrupts Water Structure Whereas Negative Charges Enhances It. *J. Phys. Chem. B* **2018**, *122*, 12260−12270.
(44) Wen, Y. C.; Zha, S.; Liu, X.; Yang, S. S.; Guo, P.; Shi, G. S.; Fang, H. P.; Shen, Y. R.; Tian, C. S. Unveiling Microscopic Structures of Charged Water Interfaces by Surface-Specific Vibrational Spectroscopy. *Phys. Rev. Lett.* **2016**, *116*, 016101.
(45) Gonella, G.; Lutgebaucks, C.; de Beer, A. G. F.; Roke, S. Second Harmonic and Sum-Frequency Generation from Aqueous Interfaces Is Modulated by Interference. *J. Phys. Chem. C* **2016**, *120*, 9165−9173.
(46) Richert, M. E.; Gochev, G. G.; Braunschweig, B. Specific Ion Effects of Trivalent Cations on the Structure and Charging State of β-Lactoglobulin Adsorption Layers. *Langmuir* **2019**, *35*, 11299−11307.
(47) Schaefer, J.; Backus, E. H. G.; Nagata, Y.; Bonn, M. Both Inter- and Intramolecular Coupling of O−H Groups Determine the Vibrational Response of the Water/Air Interface. *J. Phys. Chem. Lett.* **2016**, *7*, 4591−4595.

https://dx.doi.org/10.1021/jacs.0c11976
J. Am. Chem. Soc. 2021, 143, 1758−1762